Published in final edited form as:
Exp Neurol. 2012 July ; 236(1): 69–78. doi:10.1016/j.expneurol.2012.04.003.

Rodent neonatal germinal matrix hemorrhage mimics the human brain injury, neurological consequences, and post-hemorrhagic hydrocephalus

Tim Lekic[a], **Anatol Manaenko**[a], **William Rolland**[a], **Paul R. Krafft**[a], **Regina Peters**[a], **Richard E. Hartman**[b], **Orhan Altay**[a], **Jiping Tang**[a], and **John H. Zhang**[a,c,*]

[a]Department of Physiology, School of Medicine, Loma Linda, Calif

[b]Department of Psychology, School of Science and Technology, Loma Linda, Calif

[c]Department of Neurosurgery, School of Medicine, Loma Linda, Calif

Abstract

Germinal matrix hemorrhage (GMH) is the most common neurological disease of premature newborns. GMH causes neurological sequelae such as cerebral palsy, post-hemorrhagic hydrocephalus, and mental retardation. Despite this, there is no standardized animal model of spontaneous GMH using newborn rats to depict the condition. We asked whether stereotactic injection of collagenase type VII (0.3 U) into the ganglionic eminence of neonatal rats would reproduce the acute brain injury, gliosis, hydrocephalus, periventricular leukomalacia, and attendant neurological consequences found in humans. To test this hypothesis, we used our neonatal rat model of collagenase-induced GMH in P7 pups, and found that the levels of free-radical adducts (nitrotyrosine and 4-hyroxynonenal), proliferation (mammalian target of rapamycin), inflammation (COX-2), blood components (hemoglobin and thrombin), and gliosis (vitronectin and GFAP) were higher in the forebrain of GMH pups, than in controls. Neurobehavioral testing showed that pups with GMH had developmental delay, and the juvenile animals had significant cognitive and motor disability, suggesting clinical relevance of the model. There was also evidence of white-matter reduction, ventricular dilation, and brain atrophy in the GMH animals. This study highlights an instructive animal model of the neurological consequences after germinal matrix hemorrhage, with evidence of brain injuries that can be used to evaluate strategies in the prevention and treatment of post-hemorrhagic complications.

Keywords

Stroke; experimental; Neonatal rats; Cerebral Palsy; Mental Retardation; Neurological dysfunction; Hydrocephalus; Germinal Matrix Hemorrhage

*Correspondence to: John H. Zhang, MD, PhD, Department of Physiology and Pharmacology, Loma Linda University School of Medicine, 11041 Campus Street, Risley Hall Rm 219, Loma Linda, California, 92354, U.S.A. johnzhang3910@yahoo.com (J.H.Z.).

The authors report no conflicts of interest.

Introduction

Germinal matrix hemorrhage (GMH) is the most common neurological disorder of newborns, and is defined as the rupture of immature blood vessels within the subependymal brain tissue of the premature infant (Ballabh, 2010; Vermont-Oxford, 1993). This occurs approximately 3.5 times per 1,000 live births (Heron et al., 2010) and is an increasing socio-economic problem since both the preterm birth rates, and neonatal survival, have considerably increased over the past two decades (Shennan and Bewley, 2006). The major neurological sequelae following intraventricular extension of GMH are: cerebral palsy, post-hemorrhagic hydrocephalus (PHH) and debilitating cognitive deficits (e.g. mental retardation and academic difficulties) (Ballabh et al., 2004; Bassan et al., 2007).

Since GMH has been largely unpreventable (Bassan, 2009; Roland and Hill, 2003), and because clinical treatments are mostly inadequate (supportive)(Kenet et al., 2011), it is clinically important to develop and test novel therapeutic strategies to mitigate these devastating neurological consequences. Thus, it is necessary to characterize standardized animal models to study the spectrum of brain injuries and neurobehavioral deficits following GMH, in order that neuroprotective and preventative modalities can be adequately developed and tested for this vulnerable patient population (Ballabh et al., 2007; Chua et al., 2009; Zia et al., 2009).

GMH has been modeled using several animal species, including the rabbit, dog, sheep, rat, mouse, and pig, either by direct (needle) injection of blood into the ventricle, or by changing hemodynamic (systemic) properties, including blood pressure, circulating blood volume, serum glycerol, carbon-dioxide, osmolarity, or oxygenation levels (Balasubramaniam and Del Bigio, 2006; Georgiadis et al., 2008; Goddard et al., 1980). However, these animal models do not adequately resemble the premature neonates having GMH with respect to the etiology, neuropathology, and clinical outcomes of the disease (Aquilina et al., 2011; Aquilina et al., 2007; Balasubramaniam et al., 2006; Cherian et al., 2004; Cherian et al., 2003). Although needle insertion into the brain has inherent disadvantages of producing direct trauma to surrounding tissues, the infusion of blood has little relation to a spontaneous bleed, and the modification of hemodynamic factors leading to hypoxia, hypertension, hypercarbic, hyperosmotic, or hypervolemic states will confound the GMH-induced brain pathology. Another limitation of existing models is the cost and the special expertise required to care for and rear prematurely delivered large mammals used to model GMH. Rodent models of brain injury are relatively easy to use, maintain, inexpensive to reproduce, and their neurobehavior development has been well documented (Altman and Sudarshan, 1975). However, there is a lack of rodent model bearing neurological consequences of GMH that naturally mimics the preterm survivors of GMH.

We thus chose to administer collagenase (sterile intracerebral hemorrhage inducing agent (Rosenberg et al., 1990)) for induction of GMH, because it will cause a standardized, stereotaxically-controlled, and spontaneous rupture of the ganglionic eminence into the lateral ventricles (Lekic et al., 2011). We then asked whether the induction of GMH would be attended by significant regional brain swelling (edema), delays of neurodevelopment, increased fibrogenesis and gliosis, altered body or brain growth, and cognitive or motor deficits. Finally, we evaluated the juvenile brains to demonstrate the atrophy, ventriculomegaly, and clinical relevance of the model.

Materials and Methods

Animal Groups and General Operative Procedures

This study was conducted in accordance with the National Institutes of Health guidelines for the treatment of animals, and was approved by the Institutional Animal Care and Use Committee of Loma Linda University. Timed pregnant Sprague-Dawley rats were purchased from Harlan Laboratories, Indianapolis, IN. One hundred fifty three P7 rat pups were then randomly divided into the following groups: sham-operated (n=41), needle-control (n=18), collagenase-0.1 units (n=10), collagenase-0.3 units (n=84). Pups of both genders were subjected to the operative procedure, using aseptic technique, they were gently anesthetized with 3% isoflurane (in mixed air and oxygen), while placed prone onto a stereotaxic frame. For GMH induction, betadine first sterilized the surgical scalp area, which was then incised in the longitudinal plane to expose the skull and reveal the bregma. The following stereotactic coordinates were precisely measured from bregma: 1.8 mm (rostral), 1.5 mm (lateral), and 2.8 mm (depth) from the dura. A burr hole (1 mm) was drilled, into which a 27 gauge needle was inserted at a rate of 1 mm/min. A microinfusion pump (Harvard Apparatus, Holliston, MA) infused 0.3 units of clostridial collagenase VII-S (Sigma, St Louis, MO) through the Hamilton syringe. The needle remained in place for an additional 10 minutes after injection to prevent “back-leakage”. After needle removal, the burr hole was sealed with bone wax, the incision suture closed, and the animals were allowed to recover on a 37°C heated blanket. The entire surgery took on average 20 minutes. Upon recovering from anesthesia, the animals were returned to their dams. Needle-controls consisted of needle insertion alone without collagenase infusion.

Experiment 1: Mechanisms of Brain Injury following GMH

Animal Perfusion and Tissue Extraction

The animals were fatally anesthetized with isoflurane (≥5%) followed by cardiovascular perfusion with ice-cold PBS for hemoglobin assay, thrombin level, and immunoblot analyses. The forebrains were dissected and snap-frozen with liquid-nitrogen, then stored in −80°C freezer, before protein extractions, or spectrophotometric quantification.

Brain Water Content

The percentage of brain edema was measured using the wet-weight/dry-weight method 24 hours after GMH induction (Tang et al., 2005). Quickly following sacrifice, the brains were removed and divided. Tissue weights were determined before and after drying for 24 hours in a 100°C oven, using an analytical microbalance (model AE 100; Mettler Instrument Co., Columbus, OH) that is capable of measuring within 1.0 μg of precision. Brain edema was then finally calculated as a percentage: (wet weight - dry weight)/wet weight × 100.

Hematoma Size

The hemorrhagic injury size was quantified 24 hours after GMH induction using computer-assisted outlining of brain slices. Neonatal rats were euthanized under deep (≥5%) isoflurane anesthesia. The brains were removed and cut into slices using a 1-mm rat brain matrix. Under standardized conditions, images of the brain slices were taken with a digital camera, and then converted into a binary image for the area delineation analysis using Image J software (National Institutes of Health, Bethesda, MD). Further details have published elsewhere (Chang et al., 2011; Foerch et al., 2008).

Composite Neuroscore

The 24-hour neurological evaluation consisted of a sensorimotor value represented by the combined averages from negative geotropism, righting reflex, and grip traction test as described (Balasubramaniam et al., 2006; Cherian et al., 2003; Thullier et al., 1997). The values are expressed as percent of sham, and further procedural details are provided below (in Experiment 2).

Western Blotting

For the protein immunoblot (Lekic et al., 2011), the concentration was first determined using the DC protein assay (Bio-Rad, Hercules, CA). Samples were subjected to SDS-PAGE on 4–20% gels and then transferred to nitrocellulose membrane for 100 minutes at 100 V (Bio-Rad). The blotting membranes were incubated for 1 hour with 5% nonfat milk in Tris-buffered saline containing 0.1% Tween 20. These were then incubated overnight with the following primary antibodies: anti-Vitronectin (1:25 000; Abcam, Cambridge, MA), anti-GFAP (1:20 000; Abcam, Cambridge, MA), anti-COX2 (1:200; Cayman Chemical, Ann Arbor, MI), or anti-phospho-MTOR (1:1000; Cell Signaling Technology, Danvers, MA). The membranes were then incubated with secondary antibodies (1:1000; Santa Cruz Biotechnology, Santa Cruz, CA) and then processed with the ECL plus kit (GE Healthcare and Life Science, Piscataway, NJ). For the internal control, the same membrane was probed with an antibody against β-actin (1:1000; Santa Cruz Biotechnology, Santa Cruz, CA) after being stripped. The relative density of resultant protein immunoblot images were finally semi-quantitatively analyzed using Image J software (4.0, Media Cybernetics, Silver Spring, MD) as described (Tang et al., 2004).

Hemoglobin Assay

The spectrophotometric measurement of hemorrhagic volume was performed using well-established protocols (Choudhri et al., 1997; Tang et al., 2004). Extracted forebrain tissue was placed in glass test tubes with 3 mL of PBS, and then homogenized for 60 seconds (Tissue Miser Homogenizer; Fisher Scientific, Pittsburgh, PA). After ultrasonication for 1 minute lysed erythrocyte membranes; the products were then centrifuged for 30 minutes, and Drabkin's reagent was added (Sigma-Aldrich) into aliquots of supernatant, which reacted for 15 minutes. Absorbance, using a spectrophotometer (540 nm; Genesis 10uv; Thermo Fisher Scientific, Waltham, MA), was calculated into a hemorrhagic volume (μL) on the basis of a standard curve as routinely performed (Lekic et al., 2011).

Thrombin Assay

To measure thrombin activity in the rat brain, animals were transcardially perfused with phosphate-buffered saline at 6hr, 24hr, 10d and 21d after GMH. Brain samples were then homogenized and thrombin-specific amidolytic activity was measured using the chromogenic thrombin substrate S2238 (Anaspec, Fremont, CA) as previously described (Gong et al., 2008). The final concentration of the s2238 solution was 20mM in phosphate-buffered saline. Thrombin standards were made using rat thrombin (Sigma Aldrich, St. Louis, MO) at concentrations of 0, 1.5625, 3.125, 6.25, 12.5, 25, and 50 mU/ml. Reaction mixtures consisted of 10ul of brain sample supernatant and 1.5ul of the s2238 chromogenic substrate mixture, which were then added to 90ul of phosphate-buffered saline. Reaction mixtures were allowed to incubate for 1hr at room temperature, after which the sample absorbance were spectrophotometrically measured at 405nm.

Experiment 2: Developmental Profiles following GMH

Acquisition of developmental milestones was blindly assessed over 7 days following collagenase infusion. For negative geotropism, the time needed for complete rotation (180°)

after being placed head down on a slope (20° angle) was recorded (Thullier et al., 1997). For righting reflex, the time required for the rat pups to completely roll-over onto all four limbs after being placed on their backs was measured (Thullier et al., 1997). The maximum allotted time was 60 seconds per trial (2 trials/day) for these tests. For sensorimotor function quantification, the falling latency was recorded (60 second cut-off) following forelimb grasp of a suspended line (40 cm-length, 3 mm-diameter) as was described for grip-traction testing (Cherian et al., 2003; Lekic et al., 2011). Finally, the latency of eye-opening was blindly documented by quantifying the number of days after GMH both eye lids opened for each animal.

Craniometric Measurements

Head-size (width, height) and crown-rump (body length) measurements were performed on days 0, 1, 7, 10, 14, 21, and 28, using a Boley Gauge (Franklin Dental Supply, Bellmore, NY) as described (Saad, 1990). The head-width was measured at the anterior border adjacent to the ears, and the head-height from the posterior aspect adjacent to the mandible. Rump-to-crown measurement was the greatest cranial (rostral) to tail (caudal) extension. This craniometric ration was calculated according to the total millimeters (mm) of head circumference (surface of ellipse= pi([width]x[height])/per centimeters (cm) of body length.

Experiment 3: Neurobehavioral Evaluation at the juvenile developmental stage

Cognitive Function

The animals were assessed using a series of tests. The Morris water-maze measured spatial learning and memory on three daily blocks, as we described previously (Hartman et al., 2009; Lekic et al., 2010). The apparatus consisted of a metal pool (110cm diameter), filled with water to within 15cm of the upper edge, containing a small platform (11cm diameter) for the animal to climb onto, and swim path length was digitally analyzed by Noldus Ethovision tracking software. The cued trials (maximum of 60 sec/trial) measured general associative learning, sensorimotor abilities, and motivation to escape the water with the escape platform obviously visible from above the water's surface. The platform's location changed every other trial. The spatial trials (maximum of 60 sec/trial) measured spatial learning, with the platform submerged, hidden but discoverable. The probe trials measured spatial memory by recording time spent in the target quadrant once the platform was removed. The T-Maze assessed short-term (working) memory ability (Hughes, 2004). For each trial, the rat was placed into the stem (40 cm × 10 cm) of the T-maze and allowed to explore until either the left or right arm was chosen. Following a sequence of 10 trials, the rate of spontaneous alternation (0% = none and 100% = complete; alternations/trial) was tabulated (Fathali et al., 2010; Zhou et al., 2009). Open field data was digitally recorded for 30 minutes and subsequently analyzed by Noldus Ethovision tracking software (Hartman et al., 2009). Path length within the open-topped plastic boxes (49cm-long, 35.5cm-wide, and 44.5cm-tall) was used to measure locomotor activity.

Motor Function

The percent neurodeficit was quantified using a series of six tests measuring functional deficits (100=severe, 50=moderate, 0=none): 1) proprioceptive limb placing, 2) lateral limb placement, 3) forelimb placement, 4) postural reflex, 5) back pressure towards edge, 6) lateral pressure towards edge. These tests are routinely performed in brain-injured juvenile rats (Fathali et al., 2010; Zhou et al., 2011). The rotarod ascertained striatal ability using a standard apparatus (Columbus Instruments) consisting of a horizontal rotating cylinder (7cm-diameter × 9.5cm-wide) accelerating at 2 rpm/5 sec that requires continuous walking

to avoid falling off. Latency to fall is precisely recorded by a photobeam-circuit (Hartman et al., 2009; Lekic et al., 2010). For foot-fault testing, the number of complete limb missteps through wire-grid openings was documented per limb over 120 seconds while the animal explored an elevated wire (3 mm) suspension (20 cm × 40 cm) grid (Zhou et al., 2009).

Experiment 4: Cerebral Morphometry after one month

The animals were terminally anesthetized with isoflurane (≥5%), followed by cardiovascular perfusion with ice-cold PBS and 10% paraformaldehyde. The brains were removed and separated from surrounding tissues. The quantification of weight was performed using an analytical microbalance (model AE 100; Mettler Instrument Co., Columbus, OH) capable of 1.0μg precision (loss of brain weight has been used to estimate brain damage in juvenile animals following neonatal brain injury (Andine et al., 1990)). Brains were post-fixed in 10% paraformaldehyde then 30% sucrose (weight/volume) for 3 days. Histopathological analyses used 10 μm thick coronal sections, caudally cut every 600 μm on a cryostat (Leica Microsystems LM3050S), then mounted and stained on poly-L-lysine-coated slides. Morphometric analysis of cresyl violet slides (Lekic et al., 2011) involved computer-assisted (ImageJ 4.0, Media Cybernetics, Silver Spring, MD) hand delineation of the ventricle system (lateral, third, cerebral aqueduct, and fourth), hemisphere (cortex, subcortex), caudate, thalamus, hippocampus, and corpus callosum (white matter). The borderlines of these structures were based on criteria derived from stereologic studies using optical dissector principles (Avendano et al., 2005; Bermejo et al., 2003; Ekinci et al., 2008; Oorschot, 1996; Reisert et al., 1984; Tang et al., 2001). The volumes were calculated: [(Average [(Area of coronal section) × Interval × Number of sections) (MacLellan et al., 2008)].

Statistical Analysis

Significance was considered at $P<0.05$. Behavior data were statistically analyzed using Kruskal-Wallis one-way analysis of variance (ANOVA) on ranks, followed by the Student-Newman-Keuls Method, and repeated-measures ANOVA for long-term analyses. All other data were statistically analyzed using one-way ANOVA, followed by Tukey post-hoc test for significant analyses. Statistical analyses were performed using SigmaPlot version 10.0 for Windows.

Results

Experimental Model of Germinal Matrix Hemorrhage using Rats

All pups tolerated the procedure, recovered from anesthesia, and had a zero percent mortality rate across the entire study. The stereotaxic collagenase-induced hematoma originated from the cerebral parenchyma of ganglionic-eminence and one day later spread throughout the adjacent ipsilateral peri-ventricular brain region (Fig. 1B). Unilateral collagenase infusion caused a dose-dependent elevation of brain water, hematoma size, and neurological deficit at 24 hours after GMH induction ($P<0.05$, Fig. 1D and 1E).

Experiment 1: Mechanisms of Brain Injury following GMH

To determine whether differences exist in the presence of oxidative stress markers between the brain of neonatal pups with collagenase-induced GMH, and controls (non-GMH), we evaluated free radical adducts (4-hyroxynonenal) and a cellular content marker of nitrosative stress (3-nitrotyrosine) by semi-quantitative Western blot analyses of full-thickness brain homogenates. The optical density measurement of bands confirmed that both 4-HNE (25–60 kDa) and nitrotyrosine bands (20–75 kDa) were stronger and more dense in pups with GMH than non-GMH controls at 24 hours ($P<0.05$, Fig. 2A and 2B). We next quantified

inflammatory (COX-2) and proliferation (p-mTOR) markers by Western blot analysis, which showed the COX-2 (72 kDa) and p-mTOR (289 kDa) bands were more dense in pups at 72 hours after GMH, than in controls ($P<0.05$, Fig. 2C). Next, quantifications of blood components showed an increased level of hemoglobin (Hgb) and thrombin at 24 hours after GMH, compared with controls ($P<0.05$, Fig. 2D). The level of Hgb remained significantly elevated in brain homogenates acquired up to seven days after GMH ($P<0.05$), whereas thrombin levels were also increased (1.5- to 2-fold) at 10 days post-GMH, but compared with the non-GMH controls, the difference was not statistically significant ($p=0.051$). We then finally evaluated the time-course of gliosis-related protein expression [vitronectin (75 kDa) and GFAP (55 kDa)] at 1, 3, 10, 17, and 24 days after GMH induction. The results semi-quantitatively demonstrate peak optical density blotting of vitronectin on day 24, and GFAP on day 10, compared with non-GMH controls ($P<0.05$, Fig. 2E and 2F).

Experiment 2: Developmental Profiles following GMH

The infusion of collagenase led to significant developmental delay (post-GMH days 1–3) in negative geotropism, righting reflex, grip traction, and eye-opening, as compared with non-GMH controls ($P<0.05$, Fig. 3A–D). The head size was disproportionally increased compared to body length on days 7–14, and body weight was decreased on days 1, 14, 21, and 28, compared with intact animals ($P<0.05$, Fig. 3E and 3F).

Experiment 3: Neurobehavioral Evaluation at the juvenile developmental stage

At the fourth week following GMH, all groups demonstrated equal cued learning ability in the water-maze ($P>0.05$). During the spatial (hidden platform) trials, however, collagenase infused animals performed significantly worse than controls ($P<0.05$, Fig. 4A). In comparison, the controls performed better with each block and during the spatial memory probe ($P<0.05$, Fig. 4A, right panel). Furthermore, the T-Maze showed significant loss of ‘working’ memory ($P<0.05$, Fig. 4B). Additionally, the open field test revealed significant hyperactivity ($P<0.05$, Fig. 4C). Finally, GMH led to significant motor dysfunction, as demonstrated by the comprehensive neurodeficit scale, rotarod, and foot-fault performance evaluations ($P<0.05$, Fig. 4D–F).

Experiment 4: Cerebral Morphometry after one month

Neonatal collagenase infusion (0.3 Units) resulted in a decrease in the gross whole-brain weight of the juvenile animals, four weeks later ($P<0.05$, Fig. 5A). This is qualitatively demonstrated as a generalized ventriculomegaly and brain atrophy (Fig. 5B). Volumetric analyses showed bilateral brain tissue volume losses (total, cortical, sub-cortical), and extremely dilated ventricles ($P<0.05$, Fig. 5C and 5D). Morphometry further showed the corresponding bilateral atrophy of the caudate, thalamus, hippocampus and white-matter areas ($P<0.05$, Fig. 5E and 5F).

Discussion

Several models of perinatal hypoxia-ischemia are available and have been extensively evaluated. However, collagenase GMH in neonatal rats, causing acute brain injuries and long-term neurobehavioral and histopathological consequences, has not been studied. Our experimental model has practical significance to the human condition on a number of levels. First, the intraventricular hemorrhage in this model is morphologically similar to premature infants because the hemorrhage generally begins with the rupture of blood vessels within the germinal-matrix and, subsequently, the ependyma is broken, filling the ventricle with blood (Conner et al., 1983). Second, the development of GMH-intraventricular hemorrhage in this model is mechanistically comparable to that of GMH in premature infants, since there is a spontaneous and progressive escalation of transmural pressure, blood-vessel rupture, focal

bleeding, and re-bleeding, all leading to extremes of intracranial pressure during the first few days of preterm infant life (Conner et al., 1983; Welch, 1980). Specifically, clinical conditions like the use of high pulmonary-ventilator pressure (increased cerebral venous pressure), bicarbonate infusions (increased serum osmolarity), and diuretic administration (decreased intracranial pressure), are factors causing GMH in premature infants, due to the elevation of transmural pressures across intracerebral blood vessel walls (Ballabh, 2010). Third, the induction of GMH using a standardized and commercially-available neonatal stereotaxic frame with a Hamilton syringe, minimizes the trauma to brain parenchyma. This was previously unavoidable using the free-hand approach (Alles et al., 2010; Balasubramaniam et al., 2006), despite the use of ultrasound or MRI monitoring (Xue et al., 2003). Fourth, the induction of GMH in this collagenase model results in a robust inflammatory brain response associated with elevated levels of hemoglobin and thrombin, but without any major neurological deficits, similar to human preterm newborns. Fifth, there are a number of advantages of using the rat as an experimental animal; specifically, the brain injury, neurobehavior and histopathology are well described in the rat species (Lekic et al., 2011). Sixth, this model using rats is far less expensive, is much less labor intensive, and very readily permits survival into adulthood, compared with piglets, beagles, or rabbits (Aquilina et al., 2007; Cherian et al., 2003; Georgiadis et al., 2008; Goddard et al., 1980). Seventh, the induction of GMH with collagenase creates a slow rate of intraventricular bleed (MacLellan et al., 2008); avoiding the confounding brain injury and/or infarction resulting from increased intracerebral pressures (ICP) following rapid intraventricular infusions of relatively large blood volumes (Aquilina et al., 2007; Balasubramaniam et al., 2006; Cherian et al., 2003; Mayfrank et al., 1997). Collectively, the collagenase-induced hemorrhage in the model resembles GMH of preterm newborns both mechanistically and morphologically, which makes this a useful means to study the disease process and assess therapeutic strategies.

Animal models are needed to study the evolution of brain damage and the potential of therapeutics for recovery after GMH. In this study, we characterized a novel model of GMH by stereotaxic injection of sterile collagenase into the ganglionic eminence of newborn rats. All the rats exhibited hematomal extension into the ventricles, and therefore, this model corresponds to grade III–IV (severe) GMH as defined by clinical imaging studies in premature human infants (Papile et al., 1978). Spontaneous intraventricular hemorrhage was previously induced using glycerol to cause intracranial hypotension in prematurely born rabbits (27–30 days gestation) (Conner et al., 1983). Alternatively, the direct injection of blood into newborn dog brains was used to study the effects of acute ventricular distension upon the blood flow patterns in surrounding brain tissues (Batton and Nardis, 1987). Canine models have played an essential role in the understanding of physiologic factors predisposing to GMH (Balasubramaniam and Del Bigio, 2006). There is also a mouse model of neonatal hypoxia-ischemia that develops spontaneous (superficial) foci of bleeding, but this is unlike those clinically seen in humans (Yoshioka et al., 1989). These studies have described in detail the physiologic processes, and structural features, behind the initiation of GMH, however, have not been solely suitable to study many of the tissue reactions following neonatal hemorrhagic brain injury.

In this study, collagenase infusion into the ganglionic eminence (periventricular region) of neonatal rats produced both neonatal-early (transient) and juvenile-delayed (persistent) neurobehavioral deficits. We used negative geotropism, righting-reflex, and grip-traction testing as an assessment battery for early reflex locomotor testing. The development of locomotion (surface righting and negative geotropism) and grip-traction ability (forelimb grip traction testing) are amongst the earliest developmental motor milestones described for rats (Altman and Sudarshan, 1975; Bona et al., 1997; Westerga and Gramsbergen, 1990). The first two weeks of life (postnatal days 1–14) involve rapid changes in brain

development (Davison and Dobbing, 1966; Eayrs and Goodhead, 1959), and therefore it is likely that a cerebrovascular injury, such as spontaneous ganglionic eminence bleeding, could interrupt the developmental changes necessary for timely attainment of neurobehavioral skills. Such delays in early developmental function have been documented to be predictive of neuromotor function in premature human infants (Allen and Capute, 1989). In accordance with both the clinical presentation, and a spontaneous rabbit model of GMH, our difference in performance was significantly worsened compared to control groups (sham and needle-trauma) only during the first 1–3 days following GMH (Georgiadis et al., 2008). This timing is in contrast to those findings following rodent models of intraventricular blood infusion that found persistent sensorimotor deficits for 1–2 weeks after the initial brain insult (Aquilina et al., 2011; Balasubramaniam et al., 2006). This difference likely reflects traumatic brain injury following free-hand needle insertion, despite ultrasound or MRI monitoring (Xue et al., 2003). Here, we minimized the needle trauma injury, as evidenced by the agreement in both our histopathological and neurobehavioral outcomes, that support the efficacy of using a standardized stereotaxic technique, including frame and syringe. Further, the decreased body weight on day 1 after GMH is in agreement with losses in bodily mass 24 hours after hypoxia-ischemic brain injury in P7 rats (Chen et al., 2011), and our corresponding somatic response further confirms experimental relevance of the GMH model. Most importantly, the delayed motor and cognitive deficits found in our juvenile animals correspond to the clinical presentation of deficits after GMH in humans. These are therefore likely a reflection of the ventricular dilation, brain atrophy, and direct injury to the periventricular structures, over time, from the intraventricular extending hematoma (Balasubramaniam et al., 2006). However, since both brain atrophy and ventricular enlargement were found in this study, future work will need to further characterize the ventricle size, starting from the acute phase, so to illustrate the development of hydrocephalus in this model.

The rapid progression of developmental events following the P7 developmental stage in the rat brain has differences compared to the human term neonate, and the limitation to model GMH was reviewed by others (Cherian et al., 2003). Glial proliferation in the rat peaks in the range of P1 and P20 (compared to the 3–4 months in the human). Synaptogenesis is from P14 to P21 in the rat (2–36 months in humans) and neuronal myelination is from P10 to P50 (several years following birth in humans) (Bass et al., 1970). Although for the past thirty-years, many have considered the P7 rat equivalent to the human term neonate (Rice et al., 1981), there is evidence that P7 may represent an earlier gestation. In fact, the rat cerebral cortex at P12 to P13 corresponds to the full-term newborn human infant, with respect to the degree of maturation (Romijn et al., 1991). Additionally, serial measurements of amplitude integrated EEG in rats (aged P1 to P21) suggest that P7 is equivalent to the 30–32 week pre-term neonate, while P10 corresponds to the 40–42 week human term gestation (Tucker et al., 2009).

Using the gold-standard of cognition assessment in juvenile rodents (Morris et al., 1982), we found spatial learning and memory deficits. The ventriculomegaly, brain atrophy, and white-matter losses were together related to the juvenile-associated losses in working memory (T-maze) and increased hyperactivity in the open-field (path length). Motor deficits on the accelerating rotarod and foot-fault tests further confirm the bilateral nature of the brain injury, and along with the bilateral character of the histopathology, lend support to the theory of progressive intraventricular CSF accumulation over time, as was hypothesized by others (Cherian et al., 2003; Chua et al., 2009). Recent results using drainage, irrigation, and fibrinolytic (DRIFT) therapy [to lower the intraventricular pressure, distortion, free iron, and cytokines] have shown improvements in developmental profiles, cognitive ability, and global cerebral function following GMH in pre-term humans (Whitelaw et al., 2010). Together, our results demonstrate that delayed cognitive and motor dysfunction will occur in

this model, and future studies can evaluate novel strategies for the translation of therapeutics from-bench, to-bedside.

To date, outcomes following hydrocephalus induction have been studied primarily using the kaolin (aluminum silicate) model using rodents (Lopes Lda et al., 2009). These studies predominantly describe an obstructive form of hydrocephalus, with a lesser contribution from inflammation (e.g. arachnoiditis), reactive astrocytosis and microgliosis (Deren et al., 2010). However, the nature of this cerebral inflammatory process is different compared to that following the spontaneous entry of whole blood into the CSF (Ballabh et al., 2007). The iron released from hemoglobin in the days following brain hemorrhage will catalyze lipid peroxidation and exacerbate excitotoxicity (Wagner et al., 2003). The free-iron levels in the neonatal CSF are markedly increased for several weeks after GMH, and adding insult to injury, will enhance the formation of reactive oxygen species at a vulnerable developmental stage when antioxidant enzymes have not yet been fully established (Savman et al., 2001). Furthermore, the coagulation cascade will free thrombin, which is known to cause apoptosis in cultured neurons and astrocytes (Donovan et al., 1997). Thrombin will also activate rodent microglia to enhance glutamate receptor (rNMDA) function (Gingrich et al., 2000; Moller et al., 2000). Glutamate will be released from lysed red-blood cells (RBC) to increase local CSF levels and will, at least in part, contribute to the hematoma-related brain injury (Tang et al., 2002). As the RBC-lysis proceeds, platelets within the intraventricular clot will activate and release granules containing latent transforming growth factor (TGF)-β (Grainger et al., 1995). The elevated levels of TGF-β, within the CSF, will also have contributions of the release from the choroid plexus and recruited macrophages (Flood et al., 2001). TGF-β is a powerful stimulator of fibroblasts, leading to the increased (peri-ventricular) deposition of extracellular-matrix proteins (Bottner et al., 2000), presumptively obstructing CSF flow.

There are several potential limitations of this model. First, while the GMH collagenase model is a simple means of producing hemorrhage and is reproducible, it may cause a significant inflammatory reaction (Wang and Dore, 2007) above and beyond the blood components themselves. This related inflammation, may account for a proportion of the ventricular dilation: as comparable studies, using direct blood injection in rats, required about twice the hemorrhagic volume in order for ventricular dilation to occur in only 65% of pups (Cherian et al., 2003). Therefore, it likely differs from the cerebrovascular mechanisms producing spontaneous intracerebral hemorrhage in pre-term human neonates. Second, while the hydrocephalus is most likely due to the accumulation of a large amount blood in the ventricles, it would be difficult to separate the effects of the drugs on the blood in the ventricle, from that within the brain tissue. Third, although hydrocephalus is generally thought to occur as a result of the impairment of arachnoid villi by blood and products of coagulation, the mechanism of impairment of CSF drainage (vs. overproduction) was not considered. Fourth, whereas bleeding occurs both in the brain and into the ventricles, the cause of hydrocephalus is most likely molecules within the CSF. The actual molecules causing hydrocephalus and/or impeding drainage across the arachnoid granulations have not yet been identified. Fifth, the individual contributions from thrombin, hemoglobin, iron, and the independent role of (deactivated) collagenase, minus blood products, will need to be considered. Sixth, the role of iron-chelator and anti-thrombin drugs should be investigated independently upon evolution of both hydrocephalus and neurobehavioral difficulties. Seventh, the brain hemorrhage initiating from germinal matrix was not demonstrated. Studies will thus need to investigate early hematoma formation following collagenase infusion into the periventricular ganglionic eminence: other work, however, used a similar brain region to model GMH (Balasubramaniam et al., 2006). Eighth, while all pups tolerated the procedure, having no mortality across the entire study, this is divergent from human findings following high-grade GMH. Clinically, this brain injury leads to a much higher rate

of mortality [approximately 30–50%; (Pikus et al., 1997)]. However, a potential strength of the model is that the final outcomes are likely some combination together of collagenase and hemorrhage.

In conclusion, the present study describes a novel rat model of neurological consequences following GMH that mimics the motor deficits and ventricular dilation seen in human preterm newborns. Based on these series of experiments, future preclinical evaluations of therapeutic strategies may assess molecular mechanisms of brain injury as pertaining to the specific blood components (hemoglobin and thrombin), free-radical adducts (nitrotyrosine and 4-hyroxynonenal), inflammation (COX-2), tissue proliferation (mTOR) and gliosis (vitronectin and GFAP) markers. Study outcomes can be linked to evaluations of specific neurological ability: a) cognition (water-maze, T-maze, open-field), and/or, b) functional status (neurodeficit scale, rotarod, foot-faults). In accordance with clinical features, the histological analyses revealed bilateral atrophy and reduced white matter of the forebrain, which was further supported by acute brain injury and reactive proliferation markers. This model appears to be an attractive tool for the evaluation of therapeutic targets in the prevention and treatment of brain hemorrhage complications in preterm newborns.

Acknowledgments

Acknowledgements and Funding

Contract grant sponsor: NIH; Contract grant numbers: HD43120, NS43338, and NS54685 (to J.H.Z.).

References

1. Allen MC, Capute AJ. Neonatal neurodevelopmental examination as a predictor of neuromotor outcome in premature infants. Pediatrics. 1989; 83:498–506. [PubMed: 2927988]
2. Alles YC, Greggio S, Alles RM, Azevedo PN, Xavier LL, DaCosta JC. A novel preclinical rodent model of collagenase-induced germinal matrix/intraventricular hemorrhage. Brain Res. 2010; 1356:130–138. [PubMed: 20692236]
3. Altman J, Sudarshan K. Postnatal development of locomotion in the laboratory rat. Anim Behav. 1975; 23:896–920. [PubMed: 1200422]
4. Andine P, Thordstein M, Kjellmer I, Nordborg C, Thiringer K, Wennberg E, Hagberg H. Evaluation of brain damage in a rat model of neonatal hypoxic-ischemia. J Neurosci Methods. 1990; 35:253–260. [PubMed: 2084395]
5. Aquilina K, Chakkarapani E, Love S, Thoresen M. Neonatal rat model of intraventricular haemorrhage and post-haemorrhagic ventricular dilatation with long-term survival into adulthood. Neuropathol Appl Neurobiol. 2011; 37:156–165. [PubMed: 20819170]
6. Aquilina K, Hobbs C, Cherian S, Tucker A, Porter H, Whitelaw A, Thoresen M. A neonatal piglet model of intraventricular hemorrhage and posthemorrhagic ventricular dilation. J Neurosurg. 2007; 107:126–136. [PubMed: 18459884]
7. Avendano C, Machin R, Bermejo PE, Lagares A. Neuron numbers in the sensory trigeminal nuclei of the rat: A GABA- and glycine-immunocytochemical and stereological analysis. J Comp Neurol. 2005; 493:538–553. [PubMed: 16304625]
8. Balasubramaniam J, Del Bigio MR. Animal models of germinal matrix hemorrhage. J Child Neurol. 2006; 21:365–371. [PubMed: 16901440]
9. Balasubramaniam J, Xue M, Buist RJ, Ivanco TL, Natuik S, Del Bigio MR. Persistent motor deficit following infusion of autologous blood into the periventricular region of neonatal rats. Exp Neurol. 2006; 197:122–132. [PubMed: 16271716]
10. Ballabh P. Intraventricular hemorrhage in premature infants: mechanism of disease. Pediatr Res. 2010; 67:1–8. [PubMed: 19816235]
11. Ballabh P, Braun A, Nedergaard M. The blood-brain barrier: an overview: structure, regulation, and clinical implications. Neurobiol Dis. 2004; 16:1–13. [PubMed: 15207256]

12. Ballabh P, Xu H, Hu F, Braun A, Smith K, Rivera A, Lou N, Ungvari Z, Goldman SA, Csiszar A, Nedergaard M. Angiogenic inhibition reduces germinal matrix hemorrhage. Nat Med. 2007; 13:477–485. [PubMed: 17401377]
13. Bass NH, Netsky MG, Young E. Effect of neonatal malnutrition on developing cerebrum. II. Microchemical and histologic study of myelin formation in the rat. Arch Neurol. 1970; 23:303–313. [PubMed: 4920207]
14. Bassan H. Intracranial hemorrhage in the preterm infant: understanding it, preventing it. Clin Perinatol. 2009; 36:737–762. v. [PubMed: 19944833]
15. Bassan H, Limperopoulos C, Visconti K, Mayer DL, Feldman HA, Avery L, Benson CB, Stewart J, Ringer SA, Soul JS, Volpe JJ, du Plessis AJ. Neurodevelopmental outcome in survivors of periventricular hemorrhagic infarction. Pediatrics. 2007; 120:785–792. [PubMed: 17908766]
16. Batton DG, Nardis EE. The effect of intraventricular blood on cerebral blood flow in newborn dogs. Pediatr Res. 1987; 21:511–515. [PubMed: 3588092]
17. Bermejo PE, Jimenez CE, Torres CV, Avendano C. Quantitative stereological evaluation of the gracile and cuneate nuclei and their projection neurons in the rat. J Comp Neurol. 2003; 463:419–433. [PubMed: 12836177]
18. Bona E, Johansson BB, Hagberg H. Sensorimotor function and neuropathology five to six weeks after hypoxia-ischemia in seven-day-old rats. Pediatr Res. 1997; 42:678–683. [PubMed: 9357943]
19. Bottner M, Krieglstein K, Unsicker K. The transforming growth factor-betas: structure, signaling, and roles in nervous system development and functions. J Neurochem. 2000; 75:2227–2240. [PubMed: 11080174]
20. Chang CF, Chen SF, Lee TS, Lee HF, Shyue SK. Caveolin-1 deletion reduces early brain injury after experimental intracerebral hemorrhage. Am J Pathol. 2011; 178:1749–1761. [PubMed: 21435456]
21. Chen W, Ma Q, Suzuki H, Hartman R, Tang J, Zhang JH. Osteopontin reduced hypoxia-ischemia neonatal brain injury by suppression of apoptosis in a rat pup model. Stroke. 2011; 42:764–769. [PubMed: 21273567]
22. Cherian S, Whitelaw A, Thoresen M, Love S. The pathogenesis of neonatal post-hemorrhagic hydrocephalus. Brain Pathol. 2004; 14:305–311. [PubMed: 15446586]
23. Cherian SS, Love S, Silver IA, Porter HJ, Whitelaw AG, Thoresen M. Posthemorrhagic ventricular dilation in the neonate: development and characterization of a rat model. J Neuropathol Exp Neurol. 2003; 62:292–303. [PubMed: 12638733]
24. Choudhri TF, Hoh BL, Solomon RA, Connolly ES Jr, Pinsky DJ. Use of a spectrophotometric hemoglobin assay to objectively quantify intracerebral hemorrhage in mice. Stroke. 1997; 28:2296–2302. [PubMed: 9368579]
25. Chua CO, Chahboune H, Braun A, Dummula K, Chua CE, Yu J, Ungvari Z, Sherbany AA, Hyder F, Ballabh P. Consequences of intraventricular hemorrhage in a rabbit pup model. Stroke. 2009; 40:3369–3377. [PubMed: 19661479]
26. Conner ES, Lorenzo AV, Welch K, Dorval B. The role of intracranial hypotension in neonatal intraventricular hemorrhage. J Neurosurg. 1983; 58:204–209. [PubMed: 6848677]
27. Davison AN, Dobbing J. Myelination as a vulnerable period in brain development. Br Med Bull. 1966; 22:40–44. [PubMed: 5321813]
28. Deren KE, Packer M, Forsyth J, Milash B, Abdullah OM, Hsu EW, McAllister JP 2nd. Reactive astrocytosis, microgliosis and inflammation in rats with neonatal hydrocephalus. Exp Neurol. 2010; 226:110–119. [PubMed: 20713048]
29. Donovan FM, Pike CJ, Cotman CW, Cunningham DD. Thrombin induces apoptosis in cultured neurons and astrocytes via a pathway requiring tyrosine kinase and RhoA activities. J Neurosci. 1997; 17:5316–5326. [PubMed: 9204916]
30. Eayrs JT, Goodhead B. Postnatal development of the cerebral cortex in the rat. J Anat. 1959; 93:385–402. [PubMed: 13819134]
31. Ekinci N, Acer N, Akkaya A, Sankur S, Kabadayi T, Sahin B. Volumetric evaluation of the relations among the cerebrum, cerebellum and brain stem in young subjects: a combination of stereology and magnetic resonance imaging. Surg Radiol Anat. 2008; 30:489–494. [PubMed: 18478176]

32. Fathali N, Ostrowski RP, Lekic T, Jadhav V, Tong W, Tang J, Zhang JH. Cyclooxygenase-2 inhibition provides lasting protection against neonatal hypoxic-ischemic brain injury. Crit Care Med. 2010; 38:572–578. [PubMed: 20029340]
33. Flood C, Akinwunmi J, Lagord C, Daniel M, Berry M, Jackowski A, Logan A. Transforming growth factor-beta1 in the cerebrospinal fluid of patients with subarachnoid hemorrhage: titers derived from exogenous and endogenous sources. J Cereb Blood Flow Metab. 2001; 21:157–162. [PubMed: 11176281]
34. Foerch C, Arai K, Jin G, Park KP, Pallast S, van Leyen K, Lo EH. Experimental model of warfarin-associated intracerebral hemorrhage. Stroke. 2008; 39:3397–3404. [PubMed: 18772448]
35. Georgiadis P, Xu H, Chua C, Hu F, Collins L, Huynh C, Lagamma EF, Ballabh P. Characterization of acute brain injuries and neurobehavioral profiles in a rabbit model of germinal matrix hemorrhage. Stroke. 2008; 39:3378–3388. [PubMed: 18845808]
36. Gingrich MB, Junge CE, Lyuboslavsky P, Traynelis SF. Potentiation of NMDA receptor function by the serine protease thrombin. J Neurosci. 2000; 20:4582–4595. [PubMed: 10844028]
37. Goddard J, Lewis RM, Armstrong DL, Zeller RS. Moderate, rapidly induced hypertension as a cause of intraventricular hemorrhage in the newborn beagle model. J Pediatr. 1980; 96:1057–1060. [PubMed: 7373467]
38. Gong Y, Xi G, Hu H, Gu Y, Huang F, Keep RF, Hua Y. Increase in brain thrombin activity after experimental intracerebral hemorrhage. Acta Neurochir Suppl. 2008; 105:47–50. [PubMed: 19066081]
39. Grainger DJ, Wakefield L, Bethell HW, Farndale RW, Metcalfe JC. Release and activation of platelet latent TGF-beta in blood clots during dissolution with plasmin. Nat Med. 1995; 1:932–937. [PubMed: 7585220]
40. Hartman R, Lekic T, Rojas H, Tang J, Zhang JH. Assessing functional outcomes following intracerebral hemorrhage in rats. Brain Res. 2009; 1280:148–157. [PubMed: 19464275]
41. Heron M, Sutton PD, Xu J, Ventura SJ, Strobino DM, Guyer B. Annual summary of vital statistics: 2007. Pediatrics. 2010; 125:4–15. [PubMed: 20026491]
42. Hughes RN. The value of spontaneous alternation behavior (SAB) as a test of retention in pharmacological investigations of memory. Neurosci Biobehav Rev. 2004; 28:497–505. [PubMed: 15465137]
43. Kenet G, Kuperman AA, Strauss T, Brenner B. Neonatal IVH--mechanisms and management. Thromb Res. 2011; 127(Suppl 3):S120–122. [PubMed: 21262430]
44. Lekic T, Hartman R, Rojas H, Manaenko A, Chen W, Ayer R, Tang J, Zhang JH. Protective effect of melatonin upon neuropathology, striatal function, and memory ability after intracerebral hemorrhage in rats. J Neurotrauma. 2010; 27:627–637. [PubMed: 20350200]
45. Lekic T, Manaenko A, Rolland W, Tang J, Zhang JH. A novel preclinical model of germinal matrix hemorrhage using neonatal rats. Acta Neurochir Suppl. 2011; 111:55–60. [PubMed: 21725732]
46. Lekic T, Rolland W, Hartman R, Kamper J, Suzuki H, Tang J, Zhang JH. Characterization of the brain injury, neurobehavioral profiles, and histopathology in a rat model of cerebellar hemorrhage. Exp Neurol. 2011; 227:96–103. [PubMed: 20887722]
47. Lopes Lda S, Slobodian I, Del Bigio MR. Characterization of juvenile and young adult mice following induction of hydrocephalus with kaolin. Exp Neurol. 2009; 219:187–196. [PubMed: 19460371]
48. MacLellan CL, Silasi G, Poon CC, Edmundson CL, Buist R, Peeling J, Colbourne F. Intracerebral hemorrhage models in rat: comparing collagenase to blood infusion. J Cereb Blood Flow Metab. 2008; 28:516–525. [PubMed: 17726491]
49. Mayfrank L, Kissler J, Raoofi R, Delsing P, Weis J, Kuker W, Gilsbach JM. Ventricular dilatation in experimental intraventricular hemorrhage in pigs. Characterization of cerebrospinal fluid dynamics and the effects of fibrinolytic treatment. Stroke. 1997; 28:141–148. [PubMed: 8996503]
50. Moller T, Hanisch UK, Ransom BR. Thrombin-induced activation of cultured rodent microglia. J Neurochem. 2000; 75:1539–1547. [PubMed: 10987834]
51. Morris RG, Garrud P, Rawlins JN, O'Keefe J. Place navigation impaired in rats with hippocampal lesions. Nature. 1982; 297:681–683. [PubMed: 7088155]

52. Oorschot DE. Total number of neurons in the neostriatal, pallidal, subthalamic, and substantia nigral nuclei of the rat basal ganglia: a stereological study using the cavalieri and optical disector methods. J Comp Neurol. 1996; 366:580–599. [PubMed: 8833111]
53. Papile LA, Burstein J, Burstein R, Koffler H. Incidence and evolution of subependymal and intraventricular hemorrhage: a study of infants with birth weights less than 1,500 gm. J Pediatr. 1978; 92:529–534. [PubMed: 305471]
54. Pikus HJ, Levy ML, Gans W, Mendel E, McComb JG. Outcome, cost analysis, and long-term follow-up in preterm infants with massive grade IV germinal matrix hemorrhage and progressive hydrocephalus. Neurosurgery. 1997; 40:983–988. discussion 988–989. [PubMed: 9149257]
55. Reisert I, Wildemann G, Grab D, Pilgrim C. The glial reaction in the course of axon regeneration: a stereological study of the rat hypoglossal nucleus. J Comp Neurol. 1984; 229:121–128. [PubMed: 6490973]
56. Rice JE 3rd, Vannucci RC, Brierley JB. The influence of immaturity on hypoxic-ischemic brain damage in the rat. Ann Neurol. 1981; 9:131–141. [PubMed: 7235629]
57. Roland EH, Hill A. Germinal matrix-intraventricular hemorrhage in the premature newborn: management and outcome. Neurol Clin. 2003; 21:833–851. vi–vii. [PubMed: 14743652]
58. Romijn HJ, Hofman MA, Gramsbergen A. At what age is the developing cerebral cortex of the rat comparable to that of the full-term newborn human baby? Early Hum Dev. 1991; 26:61–67. [PubMed: 1914989]
59. Rosenberg GA, Mun-Bryce S, Wesley M, Kornfeld M. Collagenase-induced intracerebral hemorrhage in rats. Stroke. 1990; 21:801–807. [PubMed: 2160142]
60. Saad AY. Postnatal effects of nicotine on incisor development of albino mouse. J Oral Pathol Med. 1990; 19:426–429. [PubMed: 2269938]
61. Savman K, Nilsson UA, Blennow M, Kjellmer I, Whitelaw A. Non-protein-bound iron is elevated in cerebrospinal fluid from preterm infants with posthemorrhagic ventricular dilatation. Pediatr Res. 2001; 49:208–212. [PubMed: 11158515]
62. Shennan AH, Bewley S. Why should preterm births be rising? BMJ. 2006; 332:924–925. [PubMed: 16627490]
63. Tang J, Liu J, Zhou C, Alexander JS, Nanda A, Granger DN, Zhang JH. Mmp-9 deficiency enhances collagenase-induced intracerebral hemorrhage and brain injury in mutant mice. J Cereb Blood Flow Metab. 2004; 24:1133–1145. [PubMed: 15529013]
64. Tang J, Liu J, Zhou C, Ostanin D, Grisham MB, Neil Granger D, Zhang JH. Role of NADPH oxidase in the brain injury of intracerebral hemorrhage. J Neurochem. 2005; 94:1342–1350. [PubMed: 16011743]
65. Tang Y, Lopez I, Baloh RW. Age-related change of the neuronal number in the human medial vestibular nucleus: a stereological investigation. J Vestib Res. 2001; 11:357–363. [PubMed: 12446961]
66. Tang Y, Lu A, Aronow BJ, Wagner KR, Sharp FR. Genomic responses of the brain to ischemic stroke, intracerebral haemorrhage, kainate seizures, hypoglycemia, and hypoxia. Eur J Neurosci. 2002; 15:1937–1952. [PubMed: 12099900]
67. Thullier F, Lalonde R, Cousin X, Lestienne F. Neurobehavioral evaluation of lurcher mutant mice during ontogeny. Brain Res Dev Brain Res. 1997; 100:22–28.
68. Tucker AM, Aquilina K, Chakkarapani E, Hobbs CE, Thoresen M. Development of amplitude-integrated electroencephalography and interburst interval in the rat. Pediatr Res. 2009; 65:62–66. [PubMed: 18724268]
69. Vermont-Oxford. The Vermont-Oxford Trials Network: very low birth weight outcomes for 1990. Investigators of the Vermont-Oxford Trials Network Database Project. Pediatrics. 1993; 91:540–545. [PubMed: 8441556]
70. Wagner KR, Sharp FR, Ardizzone TD, Lu A, Clark JF. Heme and iron metabolism: role in cerebral hemorrhage. J Cereb Blood Flow Metab. 2003; 23:629–652. [PubMed: 12796711]
71. Wang J, Dore S. Inflammation after intracerebral hemorrhage. J Cereb Blood Flow Metab. 2007; 27:894–908. [PubMed: 17033693]
72. Welch K. The intracranial pressure in infants. J Neurosurg. 1980; 52:693–699. [PubMed: 7373397]

73. Westerga J, Gramsbergen A. The development of locomotion in the rat. Brain Res Dev Brain Res. 1990; 57:163–174.
74. Whitelaw A, Jary S, Kmita G, Wroblewska J, Musialik-Swietlinska E, Mandera M, Hunt L, Carter M, Pople I. Randomized Trial of Drainage, Irrigation and Fibrinolytic Therapy for Premature Infants with Posthemorrhagic Ventricular Dilatation: Developmental Outcome at 2 years. Pediatrics. 2010; 125:E852–E858. [PubMed: 20211949]
75. Xue M, Balasubramaniam J, Buist RJ, Peeling J, Del Bigio MR. Periventricular/intraventricular hemorrhage in neonatal mouse cerebrum. J Neuropathol Exp Neurol. 2003; 62:1154–1165. [PubMed: 14656073]
76. Yoshioka H, Iino S, Sato N, Osamura T, Hasegawa K, Ochi M, Sawada T, Kusunoki T. New model of hemorrhagic hypoxic-ischemic encephalopathy in newborn mice. Pediatr Neurol. 1989; 5:221–225. [PubMed: 2803377]
77. Zhou Y, Fathali N, Lekic T, Ostrowski RP, Chen C, Martin RD, Tang J, Zhang JH. Remote limb ischemic postconditioning protects against neonatal hypoxic-ischemic brain injury in rat pups by the opioid receptor/Akt pathway. Stroke. 2011; 42:439–444. [PubMed: 21183744]
78. Zhou Y, Fathali N, Lekic T, Tang J, Zhang JH. Glibenclamide improves neurological function in neonatal hypoxia-ischemia in rats. Brain Res. 2009; 1270:131–139. [PubMed: 19306849]
79. Zia MT, Csiszar A, Labinskyy N, Hu F, Vinukonda G, LaGamma EF, Ungvari Z, Ballabh P. Oxidative-nitrosative stress in a rabbit pup model of germinal matrix hemorrhage: role of NAD(P)H oxidase. Stroke. 2009; 40:2191–2198. [PubMed: 19372442]

Highlights

- Human neonatal germinal matrix hemorrhage can be studied using newborn rats.
- Collagenase-GMH models mTOR, COX, GFAP, and vitronectin, expression profiles.
- Levels of hemoglobin, thombin, and edema, accumulate in rodent GMH brain injury.
- Juvenile animals demonstrated dilated ventricles, cognitive, and motor disability.

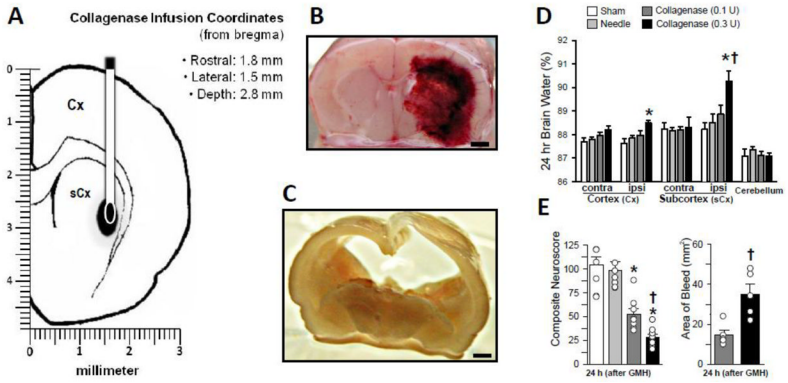

Fig. 1. Experimental Model of Germinal Matrix Hemorrhage using Rats

(A) Schematic showing stereotaxic needle placement into the ganglionic eminence near the subcortical (sCx) junction with the lateral ventricle. (B) Photomicrograph of gross coronal section 24 hours after collagenase infusion (0.3 units) illustrates hematoma localization (bar= 1 mm). (C) Coronal section of formalin perfused brain, one month after collagenase infusion (0.3 units) showing ventricular dilation (bar= 1.5 mm). (D) Degree of brain swelling, (E) Neuroscore (left), and Injury size (right). Values are expressed as mean ±SEM, n= 10 (neuroscore) and n= 5 (all others), **P*<0.05 compared with controls (sham and needle trauma), †*P*<0.05 compared with collagenase (0.1 units)

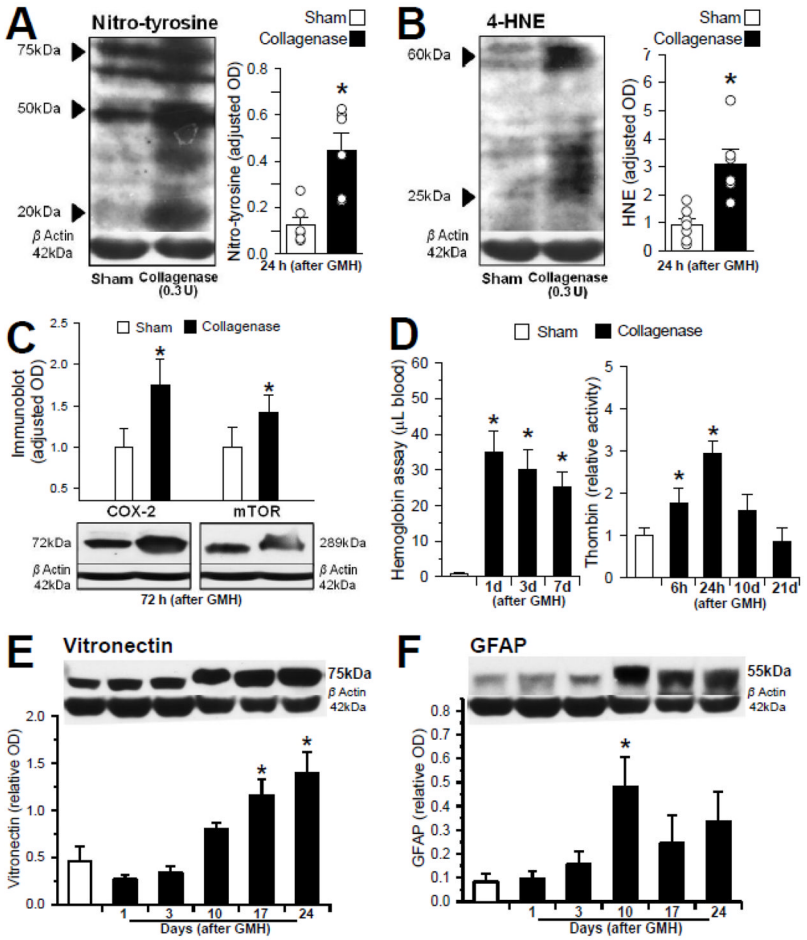

Fig. 2. Mechanisms of Brain Injury following GMH

Representative Western blot analyses at 24 hours (A,B) and 72 hours (C) post-GMH: (A) nitrotyrosine [range MW= 20–75 kDa; n=6/group], (B) 4-HNE [range MW= 25–60 kDa; n=6/group], (C) COX-2 [left, MW= 72 kDa; n=4/group] and the phosphorylated product of mTOR [right, MW= 289 kDa; n=4/group]. (D) Blood component quantification: Hemoglobin at 1, 3 and 7 days (left; n=3/group) and Thrombin at 6 and 24 hours, 10 and 21 days (right; n=4/group). Representative Western blot analysis of samples from 1 to 24 days (E) vitronectin [MW= 75 kDa; n=6/group] and (F) GFAP [MW= 55 kDa; n=6/group]. Values are expressed as mean ±SEM. **P*<0.05 compared with controls (sham and needle trauma)

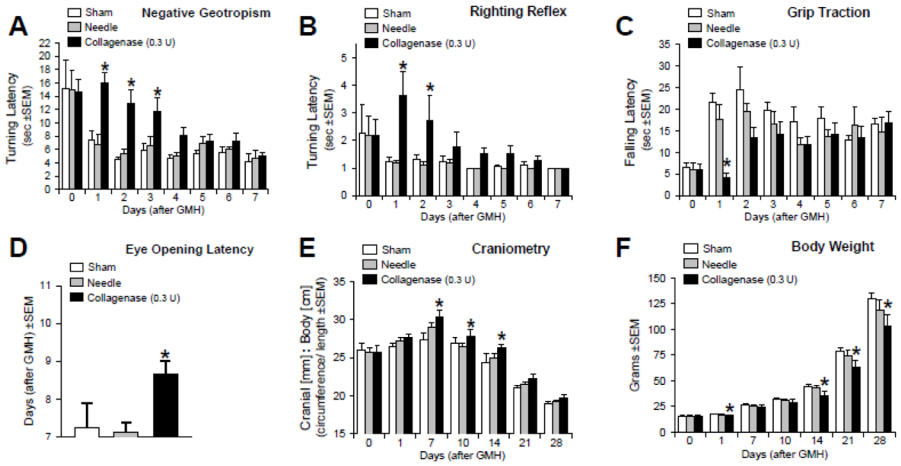

Fig. 3. Developmental Profiles following GMH

Bar graphs are demonstrating the long-term quantification of (A) Negative Geotropism, (B) Righting Reflex, (C) Grip Traction Testing, (D) Eye-Opening Latency, (E) Head Size, and (F) Body Weight. The values are expressed as mean ±SEM, n= 8 controls (sham and needle trauma), n= 9 (collagenase infusion, 0.3 units), **P*<0.05 compared with controls.

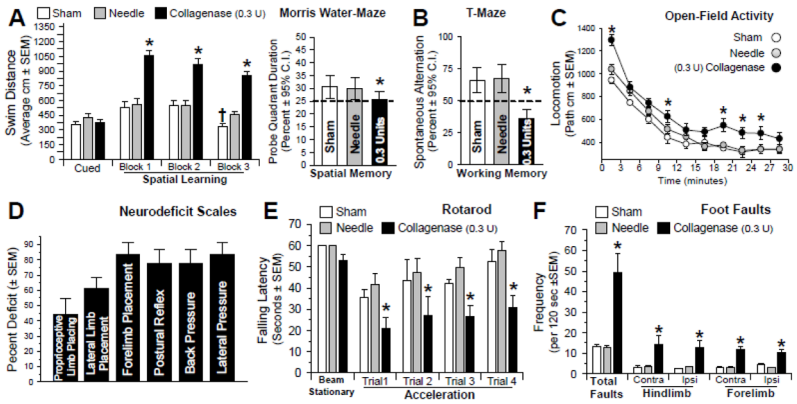

Fig. 4. Neurobehavioral Evaluation at the juvenile developmental stage

(A) Spatial learning was assessed by the swim distance needed to find the visible (cued) versus the hidden (spatial) platforms in the water-maze. (B) Spatial memory (left) was determined by the percent duration in the probe quadrant when the platform was removed. Working memory (right) was quantified by the number of spontaneous alternations in the T-Maze. (C) Level of hyperactivity was measured by the path length in open-topped boxes over a 30 minute duration. Motor function was evaluated by a battery of tests: (D) Neurodeficit Scale, (E) Rotarod, and (F) Foot Fault testing. Graphed values are expressed as mean ±SEM or mean ±95th C.I. (probe quadrant duration and alternations), n= 8 (sham and needle trauma), n= 9 (collagenase infusion, 0.3 units), **P*<0.05 compared with controls (sham and needle trauma).

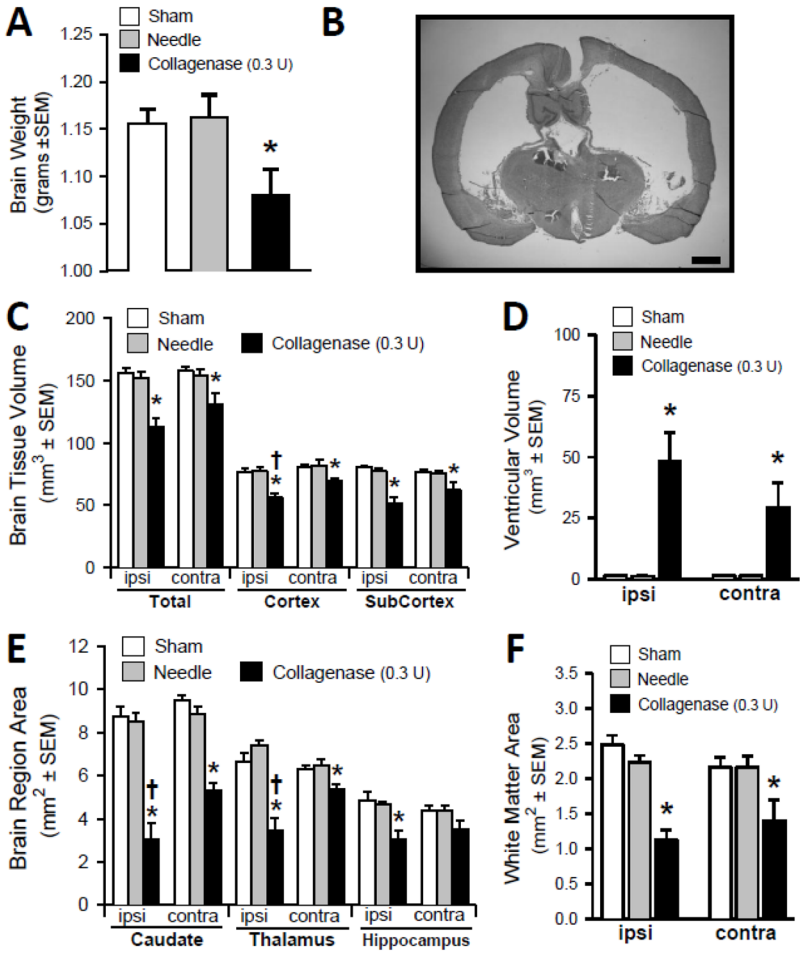

Fig. 5. Cerebral Morphometry after one month

(A) Whole-brain gross weight. (B) Representative Coronal Cryosection (scale bar= 1 mm) illustrating the bilateral ventricular dilation and overall brain atrophy. (C) Brain tissue volume (mm^3). (D) Volume of the ventricles (mm^3). (E) Subcortical brain regional areas showing atrophy. (F) White matter loss. Values expressed as mean ±SEM, n= 8 (sham and needle trauma), n= 9 (collagenase infusion, 0.3 units), *P<0.05 compared with controls (sham and needle), †P<0.05 compared with the contralateral side.